FAILURE ANALYSIS OF SKIN-STRINGER INTERFACES

B. Gómez[1], J. Reinoso*[1,2], J. Justo[1], A. Blázquez[1]

[1] *Group of Elasticity and Strength of Materials. School of Engineering, University of Seville, Camino de los Descubrimientos s/n, 41092 Seville, Spain*

[2] *Institute of Structural Analysis. Leibniz University Hannover, Appelstr. 9A, 30167 Hannover, Germany*

* *Corresponding Author: jreinoso@us.es, j.reinoso@isd.uni-hannover.de*

Keywords: Damage Mechanics, Debonding-delamination, Experimental mechanics

Abstract

Composite stiffened panels have the potentiality of producing highly efficient structures for a wide range of engineering applications. These structural conceptions are widely used in the aerospace and aeronautical industries in which optimizing the structural performance in terms of weight and safety is a recurrent objective. Based on experimental evidences, failure in these components is typically initiated at the skin-stringer interfaces and likely progressing throughout them. This work deals with the experimental analysis of a set of specimens reproducing the local geometry of a blade-stiffened panel. Two coupon typologies have been manufactured and tested following a pull-test scheme, which aimed to recreate the actual loading conditions corresponding to postbuckling symmetric anti-nodal deformation patterns.

1. Introduction

In the aerospace and aeronautical industries, the use of thin skins reinforced with stiffeners (stiffened panels) has led to produce highly efficient structures. This structural optimization trend has also promoted the incorporation of laminated composite materials for their production as a consequence of their superior specific stiffness and strength, and in this way, replacing traditional metallic materials.

Viable success of composite structures depends on the ability to fully exploit the load carrying capacity of these specimens under different loading scenarios. This aspect is of vital importance in the analysis of composite stiffened panels in postbuckling regime. However, at present, the poor understanding of the diverse failure mechanisms present in such structures has provoked to employ large reserve factors, and therefore over-sizing their design conceptions.

Experimental tests of full-scaled stiffened panels have evidenced interlaminar skin-stringer damage events as one of the main failure mechanisms responsible for the global specimen collapse [1, 2], which is usually sudden and even explosive. In this concern, damage processes generally tend to occur at the so-called nodal (locally symmetric deformed shapes) or anti-nodal (locally symmetric or antisymmetric deformed shapes) lines of the deformation pattern of the structure. In some situations, failure occur at the surface between the skin and the stringer,

whereas in other scenarios, such damage events take place at the skin or the stringer layers near the interface between both components, see [2, 3] and the references therein.

Testing full-scale composite panels have several drawbacks that regard the high costs involved, the complexity of the test rigs and the specimen instrumentation, among other aspects. Alternatively, there exists a wide set of element tests that intend to mimic the actual loading conditions of such panels along the postbuckling regime: (1) antisymmetric test, (2) pull-test, (3) push-test [4], (4) lateral tension tests [1], among others. These simplified tests usually consist of a composite single-stiffened coupon that is properly attached to a flat/curved composite skin. The way in which the external loading is applied to the specimen along with the specific geometrical definition and supporting conditions undergo the different archetypes of tests previously mentioned. One of the most appealing aspects of such simplified tests relies on the fact that they can be used to characterize the performance of the skin/stiffener interfaces, and other local phenomena, since the rest of the coupled factors that typically interact at full-scale tests are in somehow precluded.

The objective of this work concerns with the experimental analysis of the damage events that lead to the interlaminar skin-stringer failure in T-stiffened specimens by means of a pull-test configuration. Four specimen definitions were considered through the combination of two different geometry conceptions and two layup disposals.

Special attention was devoted to the analysis of the damage initiation location and progression during the tests. In this way, the importance of the geometrical characteristics and the laminate disposal in controlling the damage processes in the components is thoroughly analyzed. The experimental data reported in this work can be potentially employed for subsequent predictive numerical simulations of full-scale panels along with serving as validating database for computational models that incorporate these phenomenological aspects.

2. Specimens description: general characteristics

Two coupon typologies have been manufactured at the testing facilities of the Group of Elasticity and Strength of Materials (GERM). Based on the literature, pull-tests were chosen to characterize the critical zones at the skin-stiffener interface, using a test rig that aimed to simulate the typical symmetric postbuckling deformations along anti-nodal lines [1, 4] .

Figure 1 displays a geometrical sketch of each of the specimen types under consideration in this work. Henceforth, coupons with stretcher stringer flanges (Figure 1, on the left side) are denoted as Type-A (3 specimens for each of the laminate disposals considered), whereas the other typology (Figure 1, on the right side) are denominated as Type-B (2 specimens for each of the laminate disposals considered). Both, the skin and the stringer of every specimen were manufactured using the Carbon Fibre Reinforced Composite (CFRC) pre-preg unidirectional material IMA/M21E, whose mechanical properties are omitted here for the sake of conciseness (see [3]). The specimens were manufactured laminating two L-shaped entities corresponding to the stringer and a flat panel for the skin. At the joint between the two L-shaped entities that conform the stringer and the skin, a unidirectional fiber roll (roving) was used in order to fill the void between the different parts. Additionally, two stacking sequences have been considered for each of the components investigated (see Table 1), where, in the following, the second label used

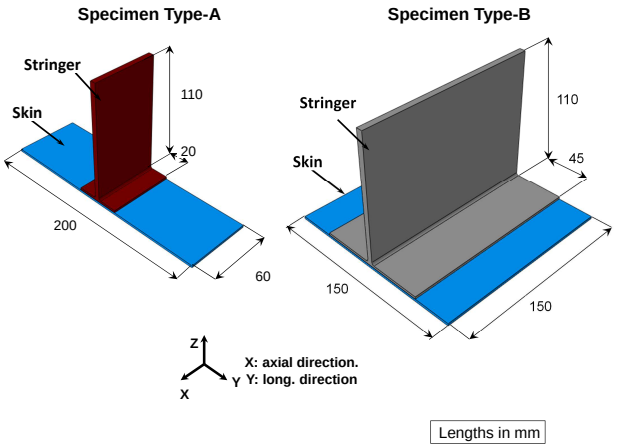

Figure 1. Geometrical definition: Type-A and Type-B specimens

Entity	Laminate 1	Laminate 2
Skin	$[45/-45/0/90/-45/45]_S$	$[45/90/-45/90/0/-45/0]_S$
Stringer	$[45/-45/0/-45/45]_S$	$[45/0/-45/0/90]_S$

Table 1. Laminate disposition Type-A and B specimens. The subscripts S denotes perfect symmetric laminate

for the identification of the laminate makes reference to this arrangement, i.e. specimen Type-A-1 refers to the stacking sequence Laminate 1 in Table 1, being analogous the denomination adopted for the rest of the specimens. The zero-degree reference direction of the laminate is identified with the x-axis of Figure 1. Thus, based on the geometrical definition and the laminate disposition, four different coupons were analyzed. Note that although the individual layouts corresponding to the skin and the stringer were symmetric, the resulting laminate of the whole specimen did not preserve this characteristic any longer.

3. Experimental program

3.1. General details

There were 10 tests under quasi-static loading conditions in total consisting of: 6 tests for the Type-A coupons (3 specimens for each layout), and 4 tests for the Type-B coupons (2 specimens for each layout). Tests were conducted at room temperature and under ambient conditions. A universal traction machine Instron 4482 was employed to carry out the experiments using two different loading cells: 5 kN for Type-A specimens and 10 kN for Type-B specimens.

Figure 2 shows the test rig, in which an auxiliary supporting system was incorporated in order to connect the specimen with the lower gripping end of the machine. An auxiliary supporting system was specifically designed and manufactured for each coupon type under study, where the longitudinal dimension corresponded to 34 mm and 20 mm in width for Type-A and Type-B specimens, respectively. The whole depth along the axial direction of each specimen was covered by this supporting system (Figure 2). Additionally, the front and rear axial edges that

conform the joint between the skin and the stringer were coloured in white in order to facilitate the detection of damage initiation and progress at these locations, see detail in Figure 2. The

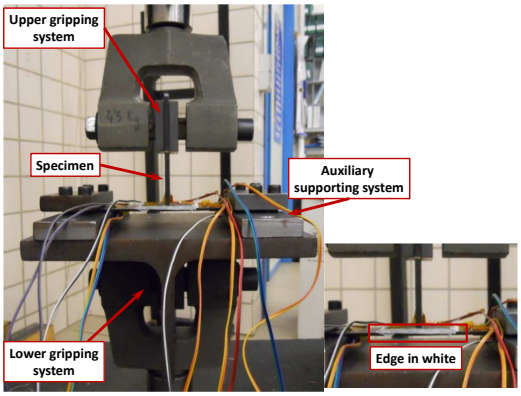

Figure 2. Test rig description

specimens responses were monitored by a set of back-to-back gages mounted at them. These data are omitted in this manuscript for the sake of brevity, although they will be included in a subsequent paper that is currently under preparation.

After testing, the coupons were visually inspected in order to determine the predominant damage mechanisms involved, along with carrying out a comparison among the experimental data recorded for each specimen type.

3.2. Experimental results: Type-A specimens

Load-displacement evolution curves of the mobile end of the testing machine corresponding to Type-A-1(1) and Type-A-2(1) specimens (the label into brackets stands for the specimen number for each of the typologies analyzed) are shown in Figure 3. Results for all Type-A specimens are reported in Table 2. Referring to the Type-A-1 coupons, a smooth evolution, preserving the linear proportionality between applied load and the deflection (A-B) was recorded until the first kink of the evolution. This variation of the response was registered to occur within the interval 1-1.2 kN for each of the specimens tested, see Table 2, and it was simultaneous with the appearance of a crack at one of the outer longitudinal extremes of the skin-stringer interface. After this, every specimen withstood higher loadings and experienced subsequent variations in the stiffness (C-D and D-E), which were consequence of: (1) further propagation of the existing damage towards the specimen center, or (2) onset of an additional damage event at the skin-stringer interface at the opposite longitudinal end of the skin-stringer interface, which only occurred for the Type-A-1(3) specimen.

A similar analysis can be performed to the experimental data corresponding to the Type-A-2 specimens. Thus, based on the deflection evolution depicted in Figure 3, it can be observed that after the initial linear evolution (A-B), the first kink in the stiffness took place at very advanced stages of the test (point B), near the maximum load level (around 1.8-2 kN). From this point until collapse, several kinks in the load-displacement evolution curves were registered. In line with the previous typology analyzed, during the tests, for every coupons, the initiation of a

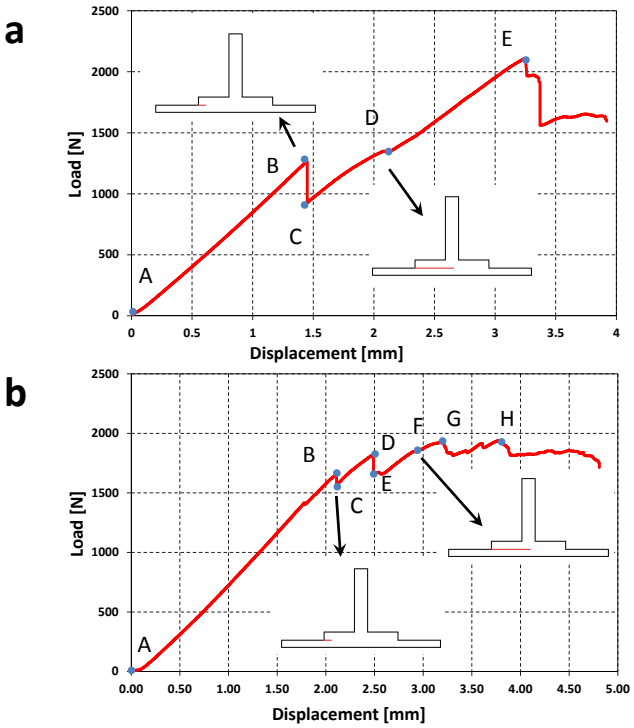

Figure 3. Load displacement evolution curves: (a) Type-A-1 specimen, (b) Type-A-2 specimen

Specimen	Crack init. load*	Final load*	Crack evol. path	Predom. dam. mech.
A-1(1)	1043	2176	From side L1-2 to centre	debond. + central delam.
A-1(2)	1200	2100	From side L1-2 to centre	debond. + central delam.
A-1(3)	1100	2800	From sides L1-2/L4-5 to centre	debond. + central delam.
A-2(1)	1600	1830	From side L1-2 to centre	debond. + diagon. delam.
A-2(2)	1700	2100	From side L1-2 to centre	debond. + diagon. delam.
A-2(3)	1555	1700	From side L1-2 to centre	debond. + diagon. delam.

Table 2. Results of the pull tests for Type-A specimens. * Crack initiation and Final loads in N

crack was detected at one of the outer longitudinal ends of the skin-stringer interface, which progressed throughout this interface, reaching the axial center underneath the roving, and after this provoking the structural collapse.

Performing a visual inspection of the fracture surfaces for both Type-A (A-1 and A-2) specimens, significant differences among them were observed, see Figure 4. Hence, whereas small delaminations were identified at the central region of the Type-A -1 coupons and the edges of the joint damage was mainly due to skin-stringer debonding, for Type-A-2 specimens, the main difference with respect to the former typology concerned the presence notable detachment of the top layer of the skin forming a diagonal mark along the central area of the surface that coincided with the material orientation of this layer.

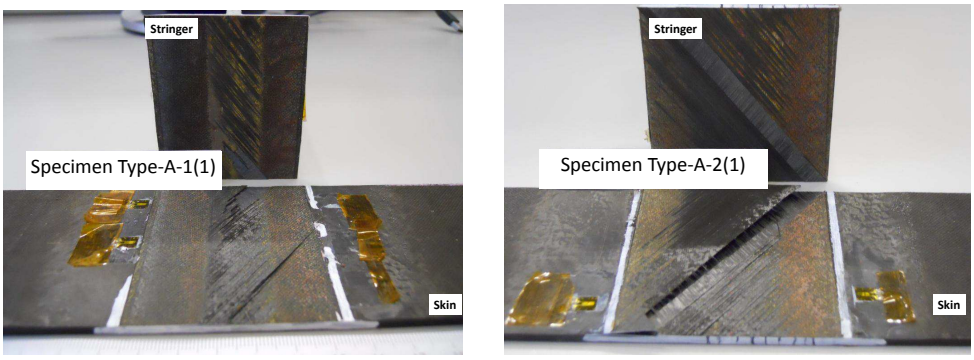

Figure 4. Fracture surfaces after test: Type-A-1(1) specimen and Type-A-2(1) specimen

Specimen	Crack init. load*	Final load*	Crack evol. path	Predom. dam. mech.
B-1(1)	6000	5270	From centre to side L1-2	debond. + diagon. delam.
B-1(2)	6500	5720	From centre to side L1-2	debond. + diagon. delam.
B-2(1)	7250	8480	From centre to side L1-2	debond. + diagon. delam.
B-2(2)	7275	5620	From centre to side L1-2	debond. + diagon. delam.

Table 3. Results of the pull tests for Type-B specimens. * Crack initiation and Final loads in N

3.3. Experimental results: specimens Type-B

Analogously to the precedent section, typical load-displacement curves corresponding to the Type-B specimens are given in Figure 5.

First, common to all the specimens tested, at point B, the most significant drop in the component stiffness was experienced at high loading levels in comparison with the collapse load. This drop is associated to the initiation of the damage, as was noticed during the experiment. However, it is observed that for Type-B-1 coupons, this sudden variation of the response occurred at lower load levels (around 6-6.5 kN, see Table 3), differing from the alternative typology (Type-B-2 specimens), for which it took place between the interval 7.250-7.275 kN. It is worth mentioning that concerning the evolution after the first peak most of the components exhibited an unstable damage propagation, since no higher load levels were achieved any longer.

In comparison to Type-A coupons, significant higher load levels were achieved for every B specimens. In addition to this, the maximum load levels recorded during the experiments were not notably affected by the different laminate disposal with the exception of the case corresponding to the Type-B-1(1) coupon that had a different response (see Table 3). In both cases, a large first stage characterized by the proportionality of the applied load was recorded (A-B in Figure 5 for both evolution diagrams).

With reference to the analysis of the fracture surfaces, as was previously highlighted, both specimen typologies B exhibited damage patterns starting from the center of the skin-stringer interface (underneath the roving) and progressing along the longitudinal direction until the ending edge of the joint. Note that this behavior completely contrasted with the performance of the specimens Type-A previously discussed.

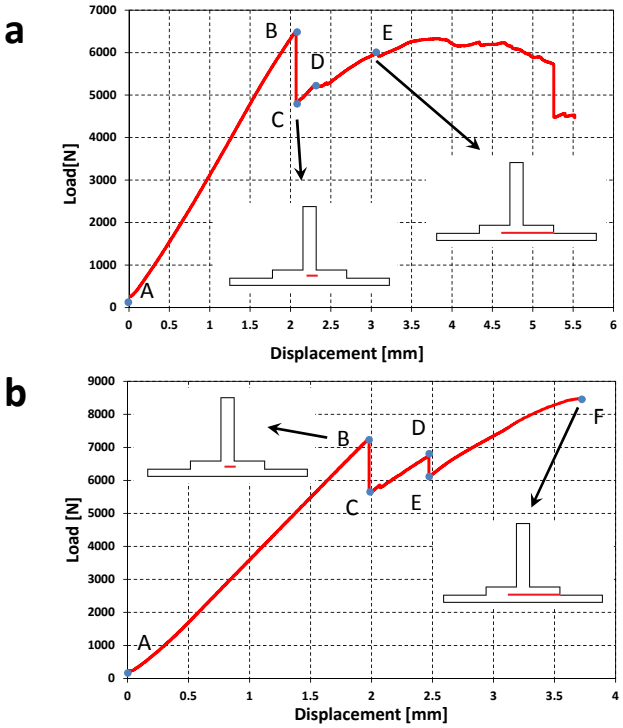

Figure 5. Load displacement evolution curves: (a) Type-B-1 specimen, (b) Type-B-2 specimen

Furthermore, performing visual inspection of failure surfaces, a common failure pattern mechanism was observed for both specimen Type-B typologies, in which two different zones were identified: (1) a central area that was characterized by the presence of significant delamination events forming 45-degrees with respect to the reference direction (Zone 1), and (2) a pair of lateral regions (at each of the axial sides of the joint) in which the predominant damage mechanisms regarded the debonding between the skin and the stringer (Zone 2).

4. Concluding remarks

This contribution outlines the pull-test analysis of two configurations of composite single stiffened panels until collapse. Failure in each test was identified as the point of first load reduction in the load-displacement evolution curves. Significant differences with regard to failure initiation and propagation paths among both coupon typologies were observed. Thus, whereas for Type-A specimens the failure at the skin-stringer interface commenced at one of the longitudinal edges of the joint and progressed towards the coupon center, for Type-B specimens, the damage was initiated underneath the roving location (at the center) and extended longitudinally towards one of the edges of the joints. Visual inspections of the damaged surface revealed: (1) the skin- stringer debonding was the predominant damage mechanism for specimens Type A-1 and A-2, where in the latter case an additional detachment of the last ply of the skin surface was observed, and (2) central delaminations and lateral skin-stringer debonding events governed the failure for both typologies of specimens Type-B.

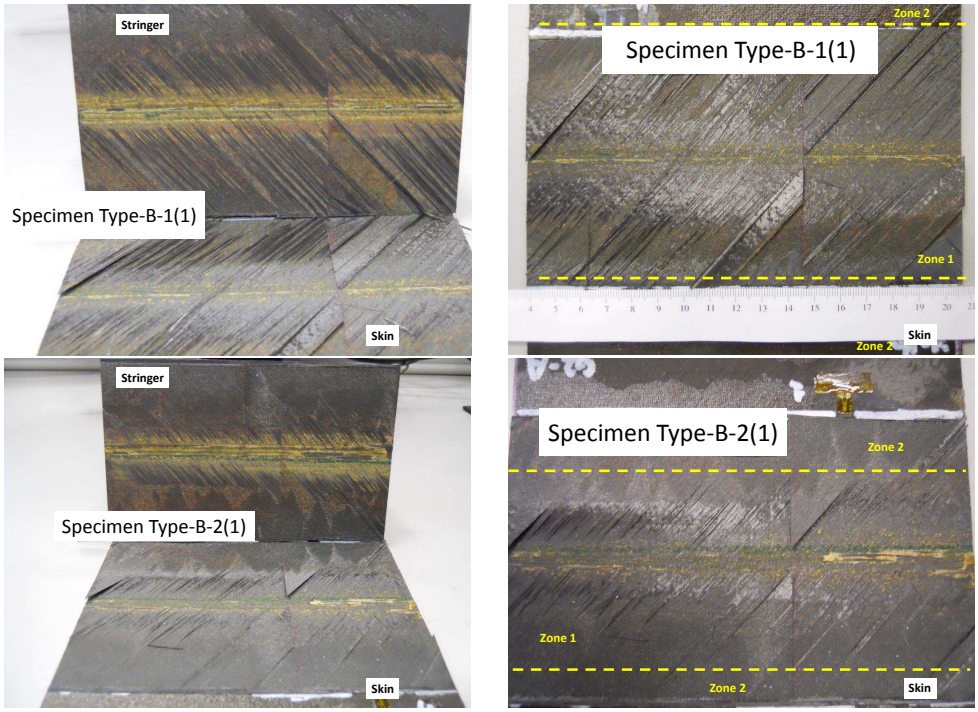

Figure 6. Fracture surfaces after test: Type-B-1(1) specimen and Type-B-2(1) specimen

Acknowledgements

This research is supported by the Ministerio de Economía y Competitividad of Spain (Project DPI2012-37187) and the Consejería de Economía, Innovación y Ciencia of Junta de Andalucía (Project TEP2011-07093).

References

[1] Meeks, C., Greenhalgh, E., Falzon, B.G. *"Stiffener debonding mechanisms in post–buckled CFRP aerospace panels"*, Composites: Part A, 36:934–946, 2005.

[2] Stevens, K.A., Ricci, R., Davies, G.A.O. *"Buckling and postbuckling of composite structures"*, Composites, 26(3):189–199, 1995.

[3] Reinoso, J., Blázquez, A., París, F., Cañas, J., Meléndez, J.C. *"Postbuckling behavior of a pressurized stiffened composite panel Part I: Experimental study"*, Composite Structures, 94(5):1533–1543, 2012.

[4] Orifici, A.C., Thomson, R.S., Herszberg, I., Weller, T., Degenhardt, R., Bayandor, J. *"An analysis methodology for failure in postbuckling skin–stiffener interfaces"*, Composite Structures, 86:186–193, 2008.